Engineering Geology 341 (2024) 107704

Contents lists available at ScienceDirect

Engineering Geology

journal homepage: www.elsevier.com/locate/enggeo

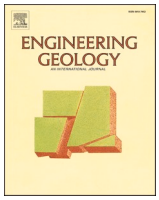

Field evidence and indicators of rockfall fragmentation and implications for mobility

Camilla Lanfranconi [a,*], Paolo Frattini [a], Federico Agliardi [a], Greg M. Stock [b], Brian D. Collins [c], Giovanni Crosta [a]

[a] Università degli studi di Milano – Bicocca, DISAT, Dept. of Earth and Environmental Sciences, Milano 20126, Italy
[b] U.S. National Park Service, Yosemite National Park, El Portal, CA 95318, United States
[c] U.S. Geological Survey, Geology, Minerals, Energy, and Geophysics Science Center, Moffett Field, CA 94035, United States

ARTICLE INFO

Keywords:
Rockfall
Rockfall fragmentation
Rockfall mobility
Rockfall talus

ABSTRACT

Rockfall fragmentation can play an important role in hazard studies and the design of protective measures. However, the current lack of modeling tools that incorporate rock fragmentation mechanics is a limitation to enhancing studies and design. This research investigates the fragmentation patterns of rockfalls and analyzes the resulting distribution of fragment sizes within corresponding rockfall deposits. We focus on small rock fragments, which provide insights into the dynamics of the rockfall event and can be used as input for numerical modeling. We analyzed multiple rockfall events from locations worldwide, each exhibiting different degrees of fragmentation. Using image analysis techniques, we mapped all visible blocks, determined their volumes, and measured the distances they travelled from the initial point of impact. A key finding is the identification of three indicators of fragmentation. First, in cases where fragmentation was largely absent, we observed a trend of increasing block size with distance from the impact point or source area, which aligns with previously published findings. However, for energetic rockfall events characterized by intense fragmentation, we observed that small fragments exhibited longer travel distances compared to larger fragments. This distinction allowed us to differentiate blocks primarily resulting from the disaggregation process from those primarily resulting from dynamic fragmentation, with implications for rockfall mobility. Second, although the size distribution of rockfall deposits exhibits a power-law scaling for volumes larger than a minimum size threshold corresponding to a rollover of the distribution, in some case studies a deviation from power-law scaling is observed, indicating a process of larger block comminution due to fragmentation. Third, we found that rockfalls with fragmentation experience reduced mobility, indicated by higher reach angles, and higher lateral dispersion showing a wider distribution of trajectories. We interpret these findings as being directly related to the energy-consuming nature of fragmentation, which prevents farther deposition of fragmented rock blocks.

1. Introduction

Rockfall events pose considerable risks to infrastructure and human safety, thus requiring the implementation of effective rockfall protection measures or other risk mitigation strategies. Understanding the behavior and characteristics of rockfalls is crucial for the design and planning of such protective measures (Agliardi et al., 2009; Volkwein et al., 2009; Lanfranconi et al., 2023). When stiff and strong rock blocks impact a hard substrate or other blocks of comparable size they may either disaggregate into smaller blocks delimited by pre-existing or latent discontinuities in the initial mass (Corominas et al., 2012; Ruiz-Carulla et al., 2018) or undergo explosive dynamic fragmentation when the involved energy exceeds a threshold (Crosta et al., 2015; De Blasio et al., 2018;). In both cases, the resulting rock fragments propagate downslope following trajectories with different dynamics compared to intact source blocks (Collins et al., 2022). This poses a substantial challenge for numerical modeling of rockfall propagation (Crosta et al., 2004; Frattini et al., 2012; Matas et al., 2017; Ruiz-Carulla et al., 2018; Sala et al., 2019).

In this paper, we analyze seven rockfall case studies, each presenting varying volumes, detachment mechanisms, energy levels, and geological and morphological settings. Rockfalls, as defined by Hungr et al. (2014),

* Corresponding author.
E-mail address: c.lanfranconi2@campus.unimib.it (C. Lanfranconi).

https://doi.org/10.1016/j.enggeo.2024.107704
Received 6 December 2023; Received in revised form 28 August 2024; Accepted 31 August 2024
Available online 2 September 2024

involve the detachment, fall, rolling, and bouncing of rock fragments. These events may occur individually or in clusters. Despite potential variability in size and scale, the defining characteristic of rockfalls lies in the minimal dynamic interaction between the most mobile fragments, which primarily interact with the substrate. Whalley (1974) introduced a size-dependent terminology, wherein debris fall, boulder fall, and block fall are individual events with volumes less than 100 m^3. As for rock avalanches, these are further distinguished from rockfalls based on a mechanical division;. Hungr et al. (2014), characterize avalanches as granular flows, suggesting that rock avalanches may originate as rockfalls but possess sufficient energy or fragmentation potential to transition into granular flows. Despite differences in size and energy levels among the case studies analyzed here, they are all categorized as rockfalls. While some events involve large volumes and energies, the classification remains consistent.

One question addressed by this study is whether rockfall fragmentation should be considered an energy-consuming process (Crosta et al., 2007; De Blasio and Crosta, 2015; De Blasio et al., 2018), or alternatively if fragmentation can enhance mobility (Jin et al., 2023) and lateral dispersion of the trajectories (Azzoni et al., 1995; Evans and Hungr, 1993; Crosta and Agliardi, 2004; Jaboyedoff et al., 2005). A second question is how dependent on contributing physical processes is characterization of rockfall block size distribution. This block size distribution exhibits nearly linear behavior in log-log space for volumes larger than case-specific thresholds (Dussauge et al., 2003; Malamud et al., 2004), whereas a downward deviation from linearity is observed for smaller volumes, indicating a censoring effect (Dussauge et al., 2003; Strunden et al., 2015). The cutoff volume is usually manually selected and guided by the shape of the distribution. Subsequently, a power-law distribution is fitted to the observed cumulative volume distribution. The block size distribution parameter is critical in assessing the hazard associated with rockfall events, as block size influences the detachment frequency (i.e., the larger the block, the smaller the frequency) and the kinetic energy (i.e., the larger the block, the higher the kinetic energy) (Hungr et al., 2014; Lari et al., 2014; Wang et al., 2014), the latter of which can entirely govern the proper selection of mitigation methods and forest protection efficiency (Lanfranconi et al., 2020). Knowledge of the block size distribution can be used to design protective structures, such as barriers and containment nets, that must be adequately sized to withstand falls of different block sizes (Dussauge-Peisser et al., 2002; Dussauge et al., 2003; Malamud et al., 2004; Lari et al., 2014; Crosta et al., 2015; Corominas et al., 2017a, 2017b; De Biagi et al., 2017). A characterization of the block size distribution requires a multi-scale method, which includes uncrewed aerial vehicle (UAV) high-resolution imagery (Carbonneau et al., 2005; Woodget and Austrums, 2017), integrated by field survey activities (Ruiz-Carulla et al., 2015).

This study aims to advance our understanding of rockfall events through detailed deposit characterization and the exploration of fragmentation indicators in frequency volume distributions. The focus is on analyzing rockfall deposits to study the distribution of blocks in the deposit containing the majority of the volume (main deposit) and the behavior of small fragments both within and outside of the main deposit. By investigating fragmentation patterns through the block size distribution and comparing it with the main deposit's distribution, our study aims to identify potentially different and distinct fragmentation behaviors. Additionally, we explore rockfall mobility using the mobility index H/L, also known as the “Fahrböschung” angle (Heim, 1932), travel angle (Cruden and Varnes, 1996), reach angle (Corominas, 1996), and travel distance angle (Hunter and Fell, 2003) among others. Here, H refers to the fall height and L refers to the horizontal length of the landslide. The H/L ratio is equivalent to the arctangent of the dipping of the line connecting the rockfall source (scar) to the most distant fallen rock block of a rockfall, and is a straightforward variable for characterizing landslide mobility (Crosta et al., 2018). Along with the mobility index, we have explored rockfall mobility through its angular representation (reach angle) and lateral dispersion (Crosta and Agliardi, 2004) to assess whether rockfall fragmentation enhances mobility or acts as an energy-consuming process, with a higher lateral dispersion indicating greater mobility in fragmented rockfalls. The findings from this study aim to enhance understanding of fragmentation to support realistic numerical simulations of rockfall runout, the assessment of risk from rockfalls, and the design of effective protection structures.

2. Case studies

We studied seven rockfall case studies characterized by differences in volumes involved, lithology, soil morphology at the impact site, and fall height (Table 1, Fig. 1). Four of the rockfalls are located in northern Italy: Villeneuve (45°42′02.8”N 7°12′29.9″E) and Saint-Oyen (45°48′59.0”N 7°12′21.0″E) in the Aosta Valley region (western Italian Alps), and Novate Mezzola (46°13′35.4”N 9°27′20.9″E) and Gallivaggio (46°21′46.8”N 9°22′08.2″E) in the Lombardy region (central Italian Alps). Another case study is located in Carcavos, in the Spanish municipality of Ayna (38°32′36.5”N 2°07′46.4”W) within the Sierra de Alcaraz domain. The remaining two case studies are the Parkline (37°40′47.5”N 119°44′54.9”W) and El Capitan rockfalls (37°43′50.4”N 119°37′33.5”W) in Yosemite National Park, California (USA), within the west-central portion of the Sierra Nevada batholith. These rockfalls capture different detachment mechanisms, energy levels, geological and morphological settings, and volumes, which provides a robust suite of case studies for exploration of fragmentation effects. Moreover, eyewitness observations of some events are available to testify as to whether or not a dynamic fractionation phenomenon has occurred.

In the Villeneuve case study (Italy, Fig. 1), approximately 650 m^3 of carbonate-silicate schist belonging to the Gran San Bernardo nappe (Penninic domain) detached during the night of 27 December 2019, destroying a rockfall barrier constructed in the late 1990s. A total volume of 15–20 m^3 reached the buildings at the foot of the slope without causing casualties. Most of the material stopped along the slope in a

Table 1
Summary data on rockfall case studies. [ITA = Italy, ES = Spain, USA = United States of America].

Rockfall event	Year of the event	Volume [m^3]	Free fall height [m]	Lithology	Eyewitness of dynamic fragmentation
Villeneuve (ITA)	2019	650	15	carbonate-silicate schist	Not available[1]
Saint-Oyen (ITA)	2020	17,500	50	micaschists	Available – no fragmentation[1]
Càrcavos (ES)	2018	260	85	limestone	Available – no fragmentation[2]
Parkline (USA)	2017	650	125	tonalite	Not available[3]
El Capitan (USA)	2017	9811	460	granite	Available –fragmentation[4]
Novate Mezzola (ITA)	2021	1080	270	granite	Not available[1]
Gallivaggio (ITA)	2018	7400	475	orthogneiss	Available – fragmentation[5]

[1] P. Frattini, Università degli Studi di Milano Bicocca, Italy, written communication, 2024.

[2] Gallo, I. G., Martínez-Corbella, M., Sarro, R., Iovine, G., López-Vinielles, J., Hérnandez, M., Robustelli, G., Mateos, R. M., & García-Davalillo, J. C. (2021). An integration of UAV-based photogrammetry and 3D modeling for rockfall hazard assessment: the Cárcavos case in 2018 (Spain). Remote Sensing, 13(17), 3450.

[3] NPS (2024)[3].

[4] Stock, G. M., Guerin, A., Avdievitch, N., Collins, B. D., & Jaboyedoff, M. (2018). Rapid 3-D analysis of rockfalls. GSA Today, 28(8), 28–29.

[5] G. Crosta, Università degli Studi di Milano Bicocca, Italy, written communication, 2024.

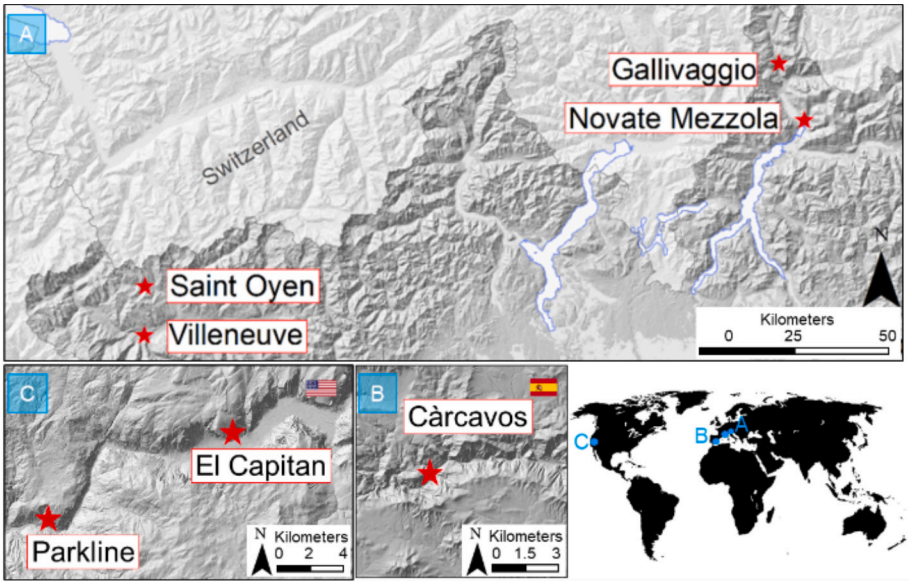

Fig. 1. Location of the rockfalls: A) Lombardy and Aosta Valley (Italy), B) Albacete province (Spain), C) Yosemite Valley (California, USA). The shaded relief images were obtained from EU-DEM (2016) for panel A), provided by IGME (2024), Spain for panel B), and provided by U.S. National Park Service (Quantum Spatial, 2020) for panel C).

generally stable condition. No eyewitness accounts of the events are available (P. Frattini, Università degli Studi di Milano Bicocca, Italy, written communication, Frattini et al., 2012).

In the Saint-Oyen case study, about 17,500 m^3 of Ruitor micaschist (Gran San Bernardo nappe) detached in March 2020, and reached a service road and playing field in the lower part of the slope, passing through a mature fir forest. No injuries were reported (Lanfranconi et al., 2023). Eyewitness accounts of the event exclude the occurrence of dynamic fragmentation (Lanfranconi et al., 2023).

Cárcavos is located in the south of the Albacete province, in the Castilla-La Mancha region of Spain (Fig. 1). The area is in the Sierra de Alcaraz, in the external zone of the Betic Cordillera (Fallot, 1948). The rockfall event that occurred on 17 November 2018, originated at the uppermost portion of a sub-vertical limestone cliff about 80 m high and involved a single 260 m^3 block. Due to impact, the block broke into more than 600 boulders of various sizes, damaging some infrastructure (Gallo et al., 2021). Eyewitness accounts of the event exclude the occurrence of dynamic fragmentation.

The 650 m^3 Parkline rockfall event (NPS, 2024) occurred in California, USA on 12 June 2017 when large exfoliation sheets of Bass Lake Tonalite detached from the cliff (Fig. 1). The rockfall source was located about 120 m above the cliff base and 180 m above El Portal Road, which

Fig. 2. Photograph of the 28 September 2017 rockfall from the southeast face of El Capitan in Yosemite Valley (photograph by Brian Degenhardt, used with permission). The huge dust cloud indicates the occurrence of fragmentation during the event.

provides a main entrance to Yosemite National Park. Rockfall debris slid down the cliff, hit a ledge, broke into many pieces and spread over 300 m, eventually reaching the Merced River below. Of the total volume of material that fell from the cliff, roughly 30 % landed on the El Portal Road, covering the road under 5–6 m of material for a linear distance of about 50 m. Most of the rock debris resulting from this rockfall was deposited along the slope above the road with the remainder located below the road. No eyewitness accounts of the events are available.

The 900 m tall southeast face of El Capitan (Fig. 1) also in Yosemite National Park, California, USA is composed predominantly of El Capitan Granite. On 27 September 2017 a series of seven rockfalls totaling 453 m^3 detached from 230 m up the southeast face of El Capitan, killing one person and seriously injuring another (Stock et al., 2018). The following day, a much larger rockfall (9811 m^3) occurred from the same location (Fig. 2). A massive slab fell from just above the previous day's rockfalls, fragmenting on impact and generating a large dust cloud. A rock fragment struck a vehicle, puncturing the sunroof and injuring the driver (Stock et al., 2018; Guerin et al., 2020). Eyewitness accounts confirm the occurrence of dynamic fragmentation evidenced by the formation of a dust cloud (Fig. 2). The presented analyses on fragmentation focus on the larger 28 September 2017 rockfall.

The Novate Mezzola village (Italy), located at the foot of Mount Avedèe, is bordered by a 500 m high cliff composed of Novate granite. In January 2021, 1080 m^3 of rock detached at an altitude of about 550 m a.s.l. Most of the material stopped at the foot of the slope and on the cliff at an elevation between 430 and 410 m a.s.l., due to the presence of a large ledge. Remaining rock blocks went over a protection embankment at the cliff foot, with some traveling far enough to damage houses located at a distance of 250–300 m from the base of the cliff. No eyewitness accounts of the events are available (P. Frattini, Università degli Studi di Milano Bicocca, Italy, written communication, Frattini et al., 2012).

The 600 m high Gallivaggio cliff (Italy) consists of a strong, stiff mylonitic orthogneiss (Truzzo granite) belonging to the Permian Truzzo pluton. On 29 May 2018, a major rockfall reached and damaged the 16th century sanctuary and surrounding buildings located at the cliff base, after passing an 8-m-high embankment and 5-m-high elasto-plastic retaining nets at the foot of the slope. The total involved volume was estimated between 6700 m^3 (Dei Cas et al., 2018; Menegoni et al., 2020) and 7400 m^3 (G. Crosta, Università degli Studi di Milano Bicocca, Italy, written communication, 2024). We use the more recent and larger estimate for the volume of this event. The rockfall produced a large dust cloud that rapidly spread and damaged a bell tower located 50 m beyond the embankment. Eyewitness accounts confirm the occurrence of dynamic fragmentation evidenced by the formation of a dust cloud.

3. Methods

The methodology adopted to investigate the signatures in the deposits of different rockfall dynamics includes: *i)* characterization of the rockfall deposit by mapping all visible blocks identified by image analysis and field observations; *ii)* calculation of the volumes of the blocks after choosing the geometric shape that fits best (since the available data often come from orthophoto images and thus when mapping in 2D the third axis size is unknown); *iii)* calculation of the distance travelled from the source area and from the main site where suspected fragmentation occurred; *iv)* calculation of the block size distribution; and *v)* calculation of mobility indexes H/L and reach angle.

Thanks to increasing resolution of orthophoto images and the availability of advanced image analysis tools, the characterization of the deposit and the mapping of visible blocks, at centimeter resolution is becoming easier. However, mapping of the deposit is highly dependent on the quality of the images, the presence of preexisting talus deposits, and the possible obstruction of trees; these issues may cause the undersampling of the smaller sized blocks.

In this study, the mapping of rock blocks was supported by UAV-sourced high resolution images for all case studies, except for El Capitan, where UAV images of the deposit were not available. Aerial photos and DTMs for the Italian case studies were provided by the associated public Italian entities (Regione Lombardia (2024) for the Gallivaggio and Novate Mezzola case studies; Regione Autonome Vallee d'Aosta (2024) for the Villeneuve and Saint-Oyen case studies) and are available by request from those agencies. The aerial photo for the Spanish case study was kindly provided by the Instituto Geológico y Minero de España (IGME) and is available upon request from that agency. Images and the DTM for the Parkline, USA case study are available from the U.S. National Park Service upon request. Aerial photos for the El Capitan, USA case study are available from the USDA (2024). For the El Capitan rockfall, the block size distribution of the main rockfall deposit was sampled in the field using a gridded clast count approach, measuring a block every 5 m along scanlines parallel to the rock wall, and spaced every 10 m. The counting of blocks was performed only on rocks without any lichen cover or weathering rinds, in order to distinguish the blocks from this rockfall from preexisting rock blocks. In the sparser deposit outside of the main deposit, we manually measured each block in the field. We georeferenced the positions of the measuring stations both within and outside the main deposit using a handheld GPS device.

For the case studies presented herein, we analyzed high-resolution post-event UAV images (Table 2) and used a semi-automatic mapping approach through the Split-Desktop software (Hexagon™) to delineate the blocks within the deposit (Fig. 3). Split-Desktop is based on a four-step 2D image processing routine: *i)* scale definition, *ii)* automatic or manual digitization of the outline of each individual block, *iii)* extraction of the particle size distribution curve, and *iv)* extraction of the two main axes of each block. Comparing to a manual mapping approach performed in GIS (assumed as more reliable), the results of this semi-automatic approach using Split-Desktop is analogous down to a specific size threshold that depends on the quality of the images available for delineating blocks. Below that threshold, the software overestimates the frequency of smaller blocks (Fig. 3). This comparison between methods allowed for the validation of the semi-automatic approach for blocks above the thresholds.

We adopted an ellipsoid shape for volume calculations, with the invisible third axes assumed to be equal to the second intermediate axis (panel 3 in Fig. 3 shows the minimum bounding geometry that we adopted to define the first two axes). More specifically, we used the rectangle of the smallest area enclosing each block polygon to calculate the maximum diameter (Walton, 1948), and then selected a volume threshold equal to 10^{-3} m^3, thereby counting only the blocks larger than that evaluated limit (Fig. 3). The shape of the blocks chosen for the case studies was validated through field surveys (in all case studies except for the Spanish one, where the ellipsoid was used for consistency and continuity with the other demos), during which random samples of blocks

Table 2
Resolution of the mapped UAV images, and number of blocks mapped within and outside the main rockfall deposit.

Rockfall event	UAV images resolution [cm/pixel]	number of blocks within the main deposit (B)	number of blocks in the distal sparse deposit (F)
Villeneuve (ITA)	2	2989	–
Saint-Oyen (ITA)	4	33,488	–
Càrcavos (ES)	3	2767	–
Parkline (USA)	6	4730	–
El Capitan (USA)	–	175 (grid by number)	1851
Novate Mezzola (ITA)	2	6678	4982
Gallivaggio (ITA)	2	18,401	38,053

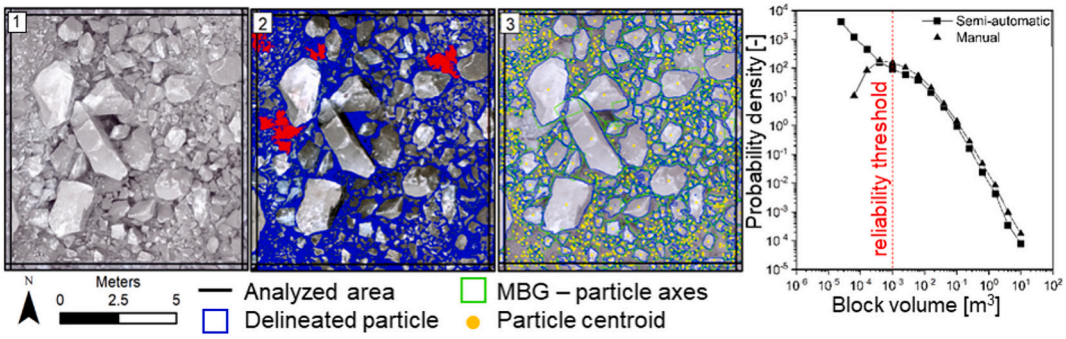

Fig. 3. Example of semi-automatic mapping approach for the Gallivaggio case study. 1) original image, 2) delineation of blocks performed by Split-Desktop software, 3) centroids and main axes obtained in GIS from the minimum bounding geometry (MGB) of the particles. Last graph on the right is a comparison between the distribution of boulder sizes delineated from the semi-automatic approach and the manual mapping approach performed in GIS for a sample area in the Gallivaggio case study. The two approaches are similar up to a reliability threshold that is a function of the quality of the analyzed image.

were collected and analyzed for their deposition characteristics. The predominance of blocks oriented with their smallest axis hidden in a 2D view validated the decision to use the ellipsoid.

Finally, we calculated the Euclidean distance of the centroid of each block (panel 3 in Fig. 3) from the base of the rockfall source wall or from the ledges or overhangs identified as the likely major impact zone from field surveys. To characterize the trend of block size with distance, we adopted the 99th percentile of volume for 10-m distance classes. This provides a means to evaluate the runout of blocks with different sizes, removing the effects of outliers from the analysis.

For the analysis of the block size distribution of the rockfall deposits, we developed non-cumulative log-binned magnitude frequency relationships, with the probability density, p, as a function of block volume, V:

$$p(V) = \frac{\partial N}{\partial V}\frac{1}{N_{tot}} \tag{1}$$

where N is the number of blocks with volume between V and V+∂A, and N_{tot} is the total number of blocks.

A power law scaling for volumes larger than a threshold is typically observed, while for smaller volumes, a downward departure from the linear behavior is observed and is typical of a censoring effect (Dussauge et al., 2003; Strunden et al., 2015). We fitted the probability density of the power-law scaling range with a Pareto distribution by using different thresholds of landslide size:

$$p(V) = \alpha c^{\alpha} V^{-(\alpha+1)}\ c > 0, \propto > 0, V \in [c, \infty) \tag{2}$$

where $\propto$, and c are the parameters of the Pareto distribution, and $\beta = \alpha + 1$ is the power-law scaling exponent of the non-cumulative distribution. The corresponding scaling exponent of the cumulative distribution would be α. We estimated the distribution parameters by a least square algorithm for different thresholds, and we selected the thresholds that maximize the fitting R^2 for each deposit.

Finally, for the analysis of rockfall mobility, we calculated the H/L ratio, which expresses the maximum vertical-to-horizontal landslide displacement ratio, and the reach angle (i.e., arctan(H/L)), and present the results in this context. Generally speaking, the reach angle can be used as an indicator of the friction coefficient that a landslide encounters during its movement (Scheidegger, 1973). A low H/L ratio indicates that the landslide travelled a long distance with a relatively small fall height.

4. Analysis and results

4.1. Distribution and density of blocks within the deposits

From the mapping of the rock block deposits, we calculated the number and resulting rock block density for each case study (Fig. 4). For the Villeneuve, Saint-Oyen, Cárcavos and Parkline sites, we observe an elongated main deposit (identified as "B"), with larger block density in the area at the foot of the slope. For the El Capitan, Novate Mezzola and Gallivaggio sites, a second, more distal, deposit (identified as "F") can be identified (Table 2). Note that the small number of blocks within the main rockfall deposit at El Capitan is due to the different sampling methodology. The slope profiles of the case studies and of the areas below the cliffs are shown in Fig. 5.

4.2. Trend of blocks size with distance

To examine the relationship between block size and distance, we analyzed the 99th percentile of block volume distribution within 10-m distance classes for each case study (Fig. 6). The 99th percentile was selected to characterize the spatial distribution of the largest blocks and was preferred to using the maximum volume in order to exclude outliers from the analysis (refer to Supplementary Fig. 1 for various percentage distributions). Some of the distance-volume trends show an exponential increase of block volume with distance and with typical rockfall deposit longitudinal sorting (Villeneuve, Saint-Oyen, Cárcavos and Parkline). Other case studies (El Capitan, Novate Mezzola and Gallivaggio) show an increase of block volume in the proximal part (direct sorting) and a decrease beyond a limit that corresponds to the edge of the proximal deposit, leading to reverse sorting. In the El Capitan case study, the limit is gradual, starting at about 360 m distance in plan from the source area (Fig. 5), whereas the limit is sharper in the Novate Mezzola and Gallivaggio case studies due to the presence of an embankment, 290 m and 300 m in plan view distance from the source area, respectively (Fig. 5). Since the evidence of reverse sorting is observed only for case studies where eyewitnesses testified to the occurrence of a considerable dust cloud, we consider this evidence as a possible indicator of fragmentation.

4.3. Frequency volume distribution

For the analysis of frequency volume distributions, we distinguished between the blocks of the main deposit of the rockfall (B in Fig. 7) and blocks/fragments mapped within the more distal and sparse deposit (F in Fig. 7) for the Gallivaggio, Novate Mezzola and El Capitan rockfalls. The limits of these two zones correspond to the distance where the trend reversal is observed (Fig. 6).

In the main deposits (B), we observe a power-law scaling for volumes larger than a threshold (red fitting line in Fig. 7), which changes in each case study, according to the quality of the mapping and a number of other physical properties such as preexisting rock fracture or discontinuity density, and intact rock material properties. This threshold is always larger than the reliability threshold used for image-analysis (V = 0.001 m^3) and varies from 10^{-2} m^3 (Novate Mezzola) to 10 m^3

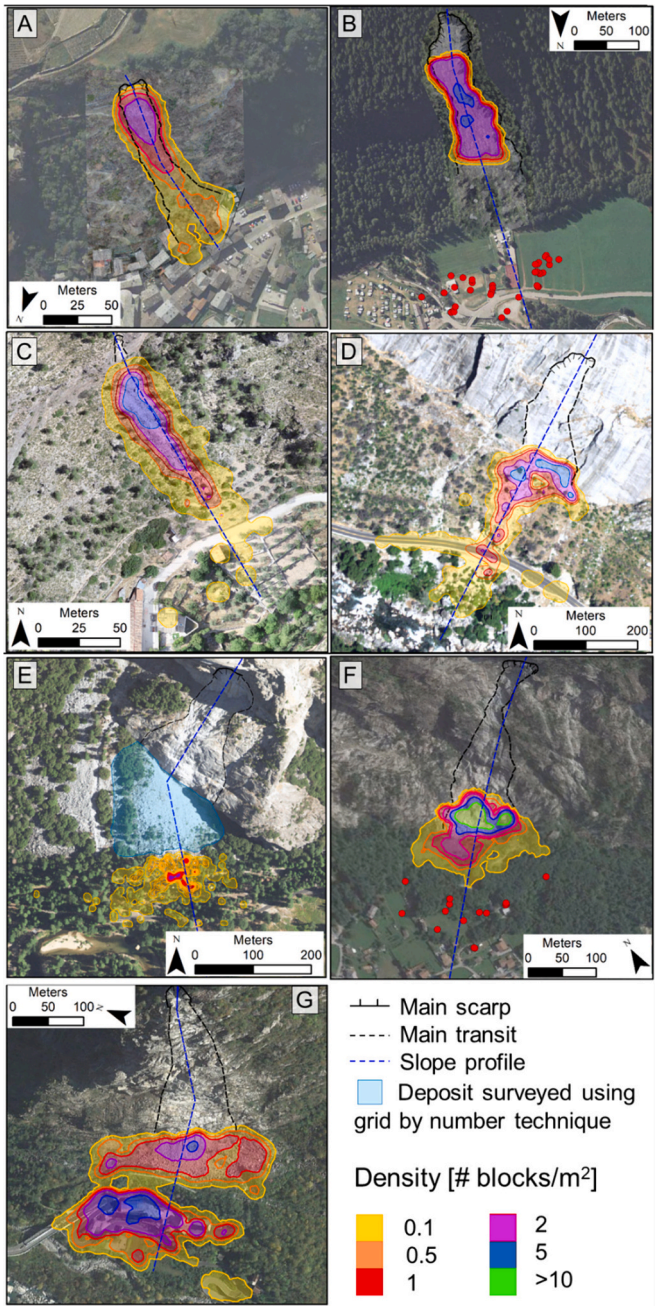

Fig. 4. Density of mapped blocks per square meter. A) Villeneuve, B) Saint-Oyen, C) Cárcavos, D) Parkline, E) El Capitan, F) Novate Mezzola, G) Gallivaggio. When few blocks occurred external to the mapped deposits, these are indicated by red dots. The density of blocks is not calculated for El Capitan main deposit due to the different mapping approach utilized. The sources of imagery presented here and utilized for analysis are provided in the Methods. (For interpretation of the references to colour in this figure legend, the reader is referred to the web version of this article.)

(Gallivaggio), with the exception of El Capitan, where the threshold is very small (10^{-3} m^3), but where the sampling methodology is not comparable with the other case studies. For the blocks/fragments (F, blue fitting line in Fig. 7) the threshold is absent (Gallivaggio and Novate Mezzola) or much smaller than the one used for the distribution obtained by image analysis. In some cases (Parkline, El Capitan, Gallivaggio, and Novate Mezzola), we also observed a deviation from the power law relationship of the frequency volume distribution of the main deposit B for block volumes larger than a second threshold, which is

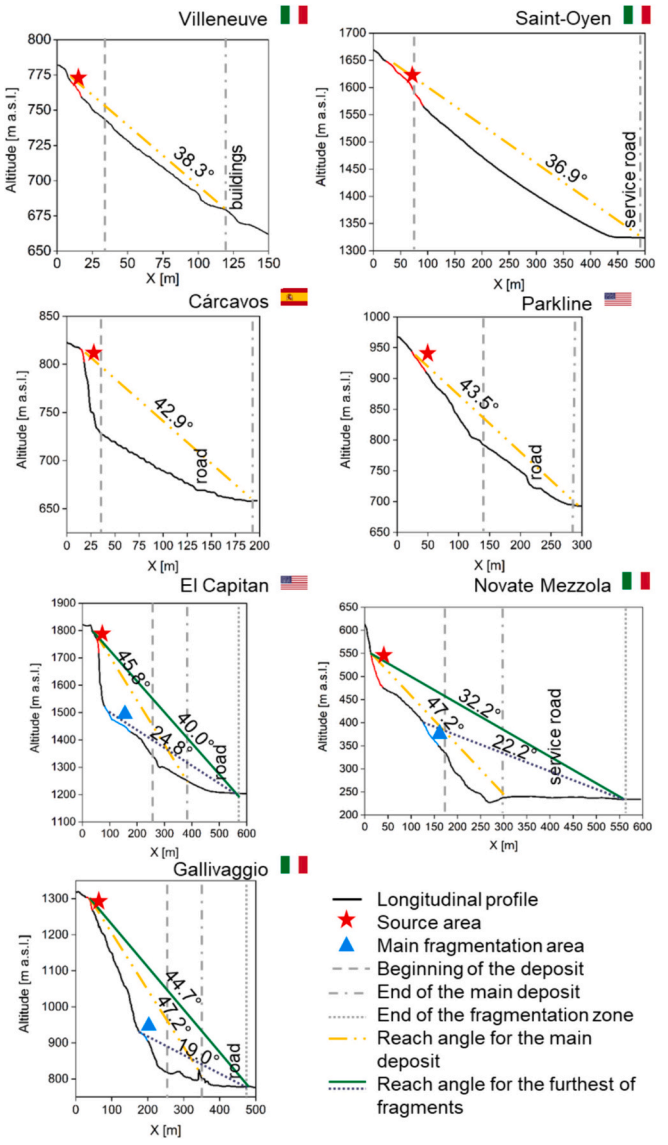

Fig. 5. Slope profiles (refer to Fig. 4 for locations), source areas, main fragmentation area and reach angles for each case study. No vertical exaggeration was applied.

approximately located between 1 and 10 m^3 (black fitting line in Fig. 7). We consider this multifractal behavior as a potential indicator of fragmentation occurrence. The scaling exponent β for all the frequency volume distributions obtained for each case study is shown in Table 3.

4.4. Rockfall mobility

4.4.1. Reach angle and H/L ratio

To examine the relationship between rockfall behavior and rockfall mobility, we plotted the elevation profiles of all the case studies and different reach angles (Fig. 5) along the profiles shown in Fig. 4. We also calculated the maximum horizontal distance reached by the farthest block of both the main deposit and the outer sparse deposit for the El Capitan, Novate Mezzola and Gallivaggio sites (Table 4; Fig. 5). For reference, typical rockfalls exhibit values of reach angle (arctan(H/L)) between 32° and 45° (Evans and Hungr, 1993). For the El Capitan, Novate Mezzola and Gallivaggio case studies, the reach angle is higher than these values when considering the main deposit, 45.8°, 47.2°, and 47.2°, respectively, but when considering the farthest fragments, decreases to 40.0°, 32.2° and 44.7° respectively (Fig. 5). The reach angle

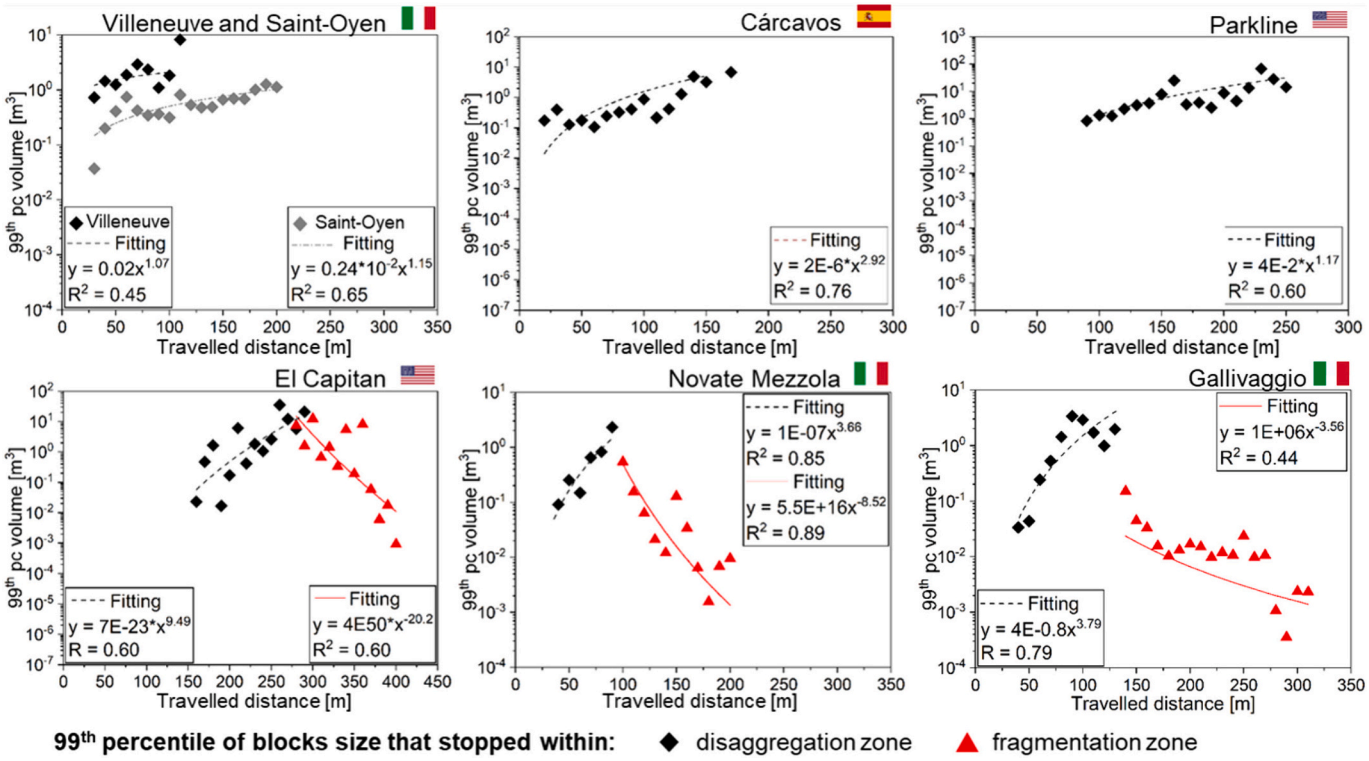

Fig. 6. Relationships between the 99th percentile of volumes of blocks within individual 10-m cells and their longitudinal travelled distance. Euclidean distances were calculated from the source area. We grouped Villeneuve and Saint-Oyen case studies in the same panel, as they belong to the same region and show similar behavior.

from the top of the fragmentation areas (i.e., the major impact point) to the furthest farthest fragments for El Capitan, Novate Mezzola and Gallivaggio is 24.8°, 22.2°, and 19.0°, respectively.

Fig. 8 shows a comparison between H/L ratio values from the literature (Scheidegger, 1973; Corominas, 1996; Wieczorek et al., 1998; Copons et al., 2009; Massey et al., 2012; Ruiz-Carulla et al., 2018) and the values of this study. Overall, we observe that the H/L values follow the same general trend from the literature. However, when only the main deposit is considered, the H/L ratio of El Capitan, Novate Mezzola and Gallivaggio are higher than expected and indicates reduced mobility.

4.4.2. *Lateral dispersion*

Another parameter that provides information about the mobility and dynamics of rockfalls is the lateral dispersion of trajectories. The path of a downslope block can deviate from the maximum slope due to rolling in concavities and oblique surface impacts, causing a disorder effect in fall paths. Moreover, clasts with asperities, characterized by any non-spherical roughness, which acquire angular momentum (spinning) during rockfall, can rebound at angles diverging from the maximum slope, even in the scenario of a perfectly smooth slope and impact medium. This effect grows with longer fall paths as the effects from variable controlling parameters spread through numerous impacts and morphological changes are encountered by the block (Crosta and Agliardi, 2004; Azzoni et al., 1995; Evans and Hungr, 1993; Jaboyedoff et al., 2005). This effect can be limited by topography. We calculated the lateral dispersion as the angle between horizontal lines that laterally bound the source area and the deposit (Fig. 9). For the main deposit (B), the angle was calculated by joining straight lines from the source area to the most lateral blocks of the deposit. For distal sparse deposits, the angle was calculated by joining the location of the fragmentation areas (Fig. 5) and the most lateral blocks of the distal deposit (Fig. 9). The results (Table 5), indicate that rockfalls characterized by fragmentation (Novate Mezzola, Gallivaggio, and El Capitan) have dispersions for [B] series in the same range as those without fragmentation whereas dispersion angles for [F] series are much higher, showing a tendency for increased lateral spreading, likely indicating more chaotic trajectories imparted during fragmentation. We consider this potential evidence for fragmentation, which, in addition to macro- and micro-topographic factors (Crosta and Agliardi, 2004), may contribute to dispersion.

5. Discussion

Rockfall fragmentation is important due to its potential effects on slope dynamics and the hazard posed by the phenomena. However, fragmentation is a complex process influenced by numerous factors including lithology, mechanical strength, debris quality, landslide height and volume, slope gradient, and morphological characteristics of the slope. Therefore, predicting the occurrence of fragmentation is extremely challenging, as is identifying fragmentation in rockfall that have already occurred. For this reason, the use of fragmentation indicators is considered relevant.

5.1. *Blocks and fragment mapping*

It is rare to recognize small fragments and other blocks outside of main rockfall deposit areas because the talus below cliff walls either already include blocks from other older events, or because the blocks stopped in forested areas are unrecognizable or too sparse. For the Gallivaggio and Novate Mezzola case studies, the areas external to the main deposit were nearly clear of pre-existing blocks and fragments and the quality of the UAV images was sufficient to allow mapping of centimeter-scale blocks and fragments. At El Capitan, although the existing talus did not permit the same level of detail in mapping the blocks of the main deposit, we achieved a high level of precision in mapping the fragments beyond the main deposit through field mapping. This was accomplished by selecting fresh rocks devoid of any lichen cover or weathering rinds, allowing us to distinguish them from

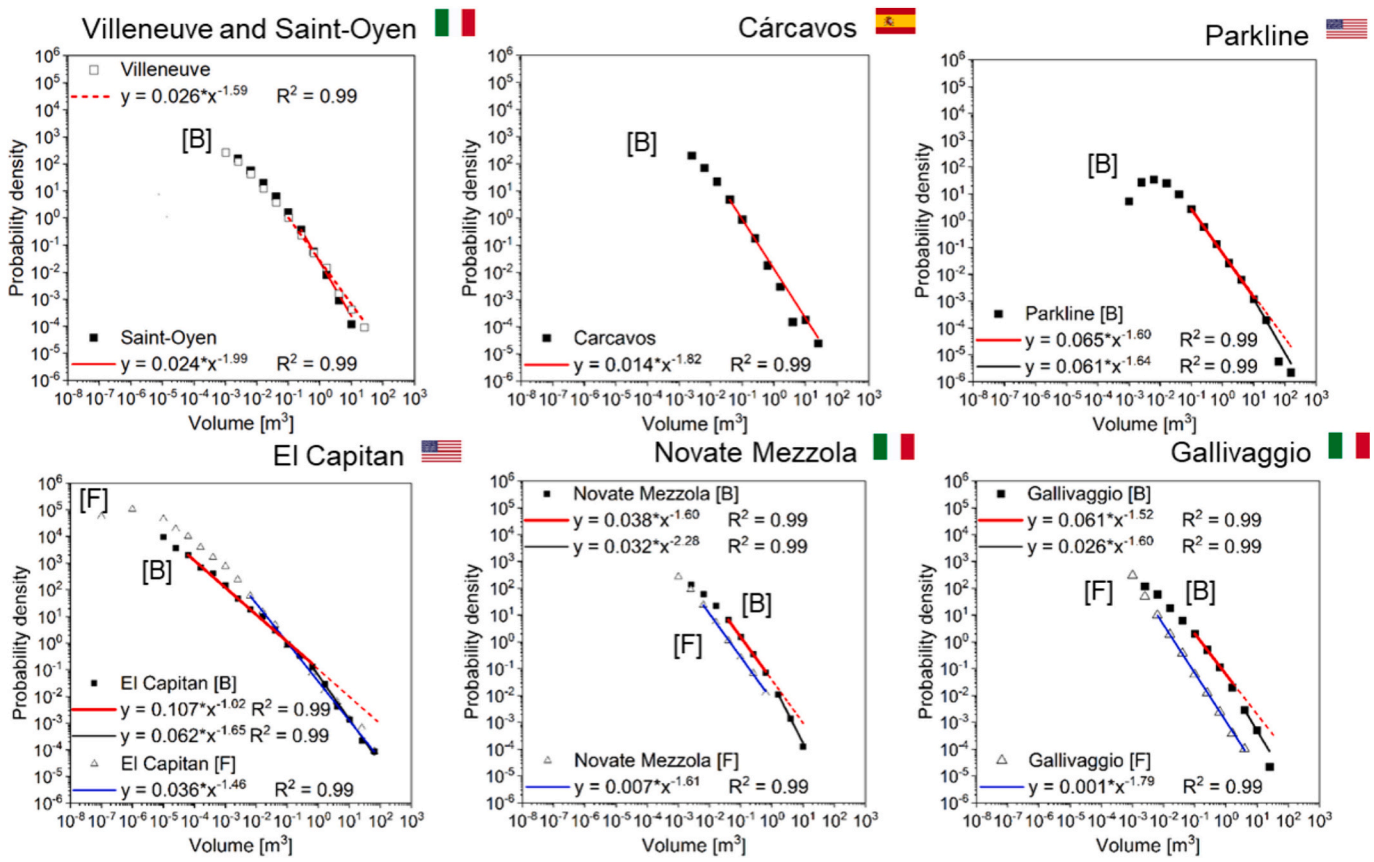

Fig. 7. Size distribution of the blocks mapped within [B] and outside [F] the main deposit. Red lines show the power-law best fit regression for the main deposits. Black lines show the power-law best fit regression for the larger blocks in the main deposits. Blues lines show the power-law best fit regression for the blocks in the more distal and sparse deposits. For the Novate Mezzola case study, the [F] series also contain the intermediate blocks. El Capitan [B] series data are less numerous because of the adopted mapping techniques (gridded clast count). The number of mapped blocks for each case study is reported in Table 2. We grouped Villeneuve and Saint-Oyen case studies in the same panel, as they belong to the same region and show similar behavior. (For interpretation of the references to colour in this figure legend, the reader is referred to the web version of this article.)

Table 3
Scaling factors β that characterize each curve in Fig. 7, and additional data on rockfall case studies.

Rockfall event	β exponent for [B] (red fitting line)	β exponent for [B] larger blocks (black fitting line)	Exponent β for [F] (blue fitting line)
Villeneuve (ITA)	1.59	–	–
Saint-Oyen (ITA)	1.99	–	–
Cárcavos (ES)	1.82	–	–
Parkline (USA)	1.60	1.64	–
El Capitan (USA)	1.02	1.65	1.46
Novate Mezzola (ITA)	1.60	2.28	1.61
Gallivaggio (ITA)	1.52	1.60	1.79

preexisting rock blocks. These distal features of some rockfall deposits are relevant because even sparsely distributed rockfall fragments can pose risk to people and infrastructure and should be taken into consideration. These less easily recognized distal features also help to define the dynamics of the rockfall event. The climatic conditions at the time of the event are also relevant, especially in the case of deep snow at the base of the cliff, which could potentially cover the ground surface and would dampen the impact, precluding the fragmentation phenomenon,

Table 4
H/L ratio and maximum distances travelled by blocks within and outside the main fragmentation zone.

Rockfall event	H/L for [B]	H/L for [B + F]	Reach Angle [B]	Reach Angle [B + F]	Maximum distance travelled block within the main rockfall deposit [m]	Maximum distance travelled for block outside the main rockfall deposit [m]
Villeneuve (ITA)	0.79	–	38.3	–	130	–
Saint-Oyen (ITA)	0.75	–	36.9	–	450	–
Cárcavos (ES)	0.93	–	42.9	–	170	–
Parkline (USA)	0.95	–	43.5	–	250	–
El Capitan (USA)	1.03	0.84	45.8	40.0	360	460
Novate Mezzola (ITA)	1.08	0.63	47.2	32.2	290	490
Gallivaggio (ITA)	1.08	0.99	47.2	44.7	300	530

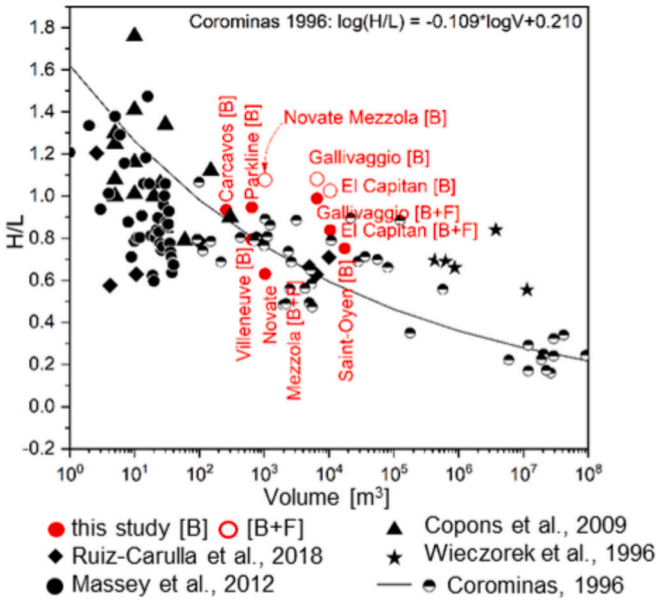

Fig. 8. Comparison between literature data (black symbols) and the case studies presented herein (red circles). Diamonds are from Ruiz-Carulla et al., 2018, triangles from Copons et al., 2009, black circles from Massey et al., 2012, stars from Wieczorek et al., 1998, and half black circles from Corominas, 1996. Fitting line from Corominas, 1996. (For interpretation of the references to colour in this figure legend, the reader is referred to the web version of this article.)

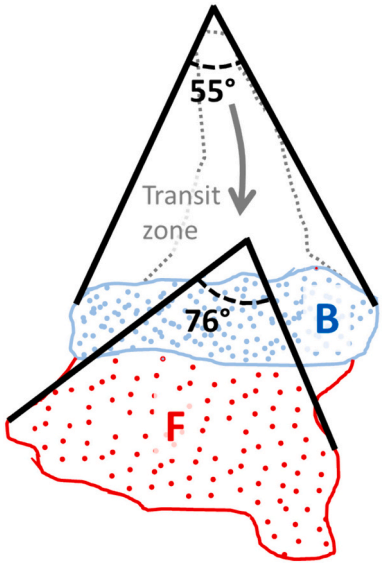

Fig. 9. Schematic representation of the Gallivaggio rockfall, with the main deposit (B) and the distal sparse deposit (F). The lines bounding the lateral dispersion of the main deposit B and the sparse deposit F are represented, defining the dispersion angles.

and in some cases control the block dynamics.

5.2. Fragmentation and block size distribution

As expected from the literature (Hantz et al., 2021), the frequency volume distribution of blocks follows power law scaling for volumes larger than a threshold (Fig. 7). In our study, we found that the scaling exponents were larger for the distal deposits (F) compared to that of all blocks in the main deposit (B). In certain cases, the scaling exponent β of blocks in the main deposit changes for larger volume blocks. This occurs especially for the Novate Mezzola and Gallivaggio rockfalls that have been subjected to a process of energetic fragmentation, as witnessed by fragments far beyond the main deposit. We interpreted this behavior as a direct recognizable effect of fragmentation, which reduces blocks larger than a certain size into smaller fragments characterized by ballistic trajectories and high velocity. In fact, the more intense the fragmentation, the more abrupt the change (i.e., Gallivaggio). Therefore, the volume where the scaling exponent changes can be interpreted as the minimum volume at which volume fragmentation is effective. A small change in the exponent for larger blocks was also observed for the Parkline event, indicating that fragmentation may also have occurred in this case study, although to a lesser extent compared to other cases. However, at Parkline it was impossible to clearly recognize a distal deposit of rock fragments because the possible fragmentation would have occurred closer to the rockfall source area, and the related fragments would have been masked by the main deposit itself. Fragmentation also occurred within the main talus slope at El Capitan, but here the extent of fragmentation observed during the event was huge, and clearly visible in the change of the exponent for larger blocks.

Table 5
Planimetric lateral dispersion observed for the different case studies.

	Lateral dispersion for [B]	Lateral dispersion for [F]
Villeneuve (ITA)	49°	–
Saint-Oyen (ITA)	25°	–
Càrcavos (ES)	41°	–
Parkline (USA)	66°	–
El Capitan (USA)	35°	58°
Novate Mezzola (ITA)	37°	101°
Gallivaggio (ITA)	55°	76°

5.3. Fragmentation and block size distribution with distance

As shown in Fig. 6, we observe two different trends in the relationship between distance and block volume for different case studies. Some events show an exponential increase in block volume with distance, indicating typical rockfall deposit longitudinal sorting (Rapp, 1960). However, other curves demonstrate a direct sorting pattern with increasing volume in the proximal part of the deposit followed by a decrease beyond a certain distance, resulting in reverse sorting. The latter behavior occurs for rockfalls that were subjected to intense dynamic fragmentation, as confirmed by eyewitnesses and by the formation of dust powder clouds (De Blasio et al., 2018). This trend reversion is interpreted as a transition between a main deposit that exhibits longitudinal sorting, and a more distal and sparse deposit that shows a reverse sorting and derives from a process of dynamic fragmentation. Therefore, we propose this reversion of the block size trend with distance may be used as a reliable indicator of fragmentation for rockfalls lacking direct observations. However, the mapping of the deposit, including blocks and fragments in the more dispersed areas, through image analysis is a time-consuming task. Image analysis can also be hampered by poor image resolution, thick vegetation cover, or local disturbances.

5.4. Fragmentation and rockfall mobility

The process of fragmentation and the mobility of rockfalls vary depending on the type of event, particularly when discussing rockfalls versus rock avalanches. A commonly used distinction is based on a mechanical division described by Hungr et al. (2014), which recognizes that rock avalanches may originate as rockfalls but, possessing sufficient energy (due to fall height) or fragmentation potential (due to rock material properties), are able to transition into granular flows. According to this distinction, we infer that perhaps the El Capitan, Novate Mezzola, and Gallivaggio events were at a transitional threshold to becoming

avalanches, but rock material properties or lack of energy hindered true flow-like behavior, and thus we still consider them as rockfalls. Additionally, the fragmentation process in rock avalanches is a highly debated subject in the scientific literature. Some researchers believe that fragmentation acts as an energy sink, resulting in a shorter mean travel distance (Crosta et al., 2007; Haug et al., 2016; Locat et al., 2006), whereas others argue that it can introduce new mechanical processes that increase mobility (Davies et al., 1999; Davies and McSaveney, 2009; De Blasio and Crosta, 2015; Zhao et al., 2017; Jin et al., 2023). Rockfalls, however, are impulsive phenomena and behave distinctly differently thanrock avalanches. What we observe empirically from our case studies is that rockfall events show a trend reversal in the relationship between distance and block volume and have high H/L ratios and reach angles that indicate less mobility due to energy consumption by fragmentation. This lower mobility is partially compensated by the ejection of fragments out of the main deposit, which in some cases may reach long distances, as at the Novate Mezzola and El Capitan sites, resulting in a much larger mobility compared to the main deposit. Also, the analysis of lateral dispersion of the trajectories shows a larger lateral spreading when fragmentation occurs. This is not related to an increase of mobility, but to the large aperture of the cone of fragmentation at impact.

5.5. Identification of fragmentation from post-event field evidence

We can summarize the results obtained from our analysis of field evidence presented herein by looking at several characteristics that may allow detection of rockfall fragmentation: i) the trend reversion of block size with distance; ii) the multifractal behavior in the frequency-volume distribution; and iii) the lateral-dispersion increase of the trajectories. The Villeneuve, Saint-Oyen and Cárcavos case studies do not show evidence of these features of fragmentation, confirming field observations, whereas the El Capitan, Novate Mezzola and Gallivaggio case studies show all the indicators of fragmentation (Table 6). The Parkline case study shows a multifractal behavior in the frequency-volume distribution (Fig. 7), with a deviation from power law, and a larger lateral dispersion than would be otherwise expected. However, Parkline completely lacks a trend reversion. We believe that these indicators are innovative in enabling post-event analysis of rockfall dynamics.

6. Conclusions

Detailed characterization of rockfall deposits can substantially advance our understanding of rockfall processes. We showed that a trend reversion in the longitudinal distribution of block size within a rockfall deposit can reveal whether dynamic fragmentation has occurred during propagation. In particular, we propose that the transition from the typical longitudinal sorting (where larger blocks travel farther due to higher energy and inertia, and less effect of deposit roughness) to reverse sorting (where smaller fragments travel farther) is indicative of dynamic fragmentation. This is clear in plots of block volume versus longitudinal distance, where dynamic fragmentation can be recognized by a rollover of the distribution of the 99th percentiles of block volumes. An additional indicator of fragmentation identified by our study is the multifractal behavior in the frequency-volume distributions of blocks and fragments. The size distribution of the main deposit without fragmentation shows a typical behavior, with a power-law scaling for volumes larger than a threshold. However, where fragmentation is suspected, most of the case studies showed a second deviation from the power law for larger volumes, which we hypothesize as the effect of fragmentation of the largest blocks. If this interpretation is correct, this second rollover may indicate a characteristic size for which fragmentation becomes effective.

Finally, we found that fragmentation can also be distinguished by typical rockfall mobility indices such as the H/L ratio, reach angle, and lateral dispersion metrics. The reach angles of rockfalls known to have experienced fragmentation at three of our case studies (El Capitan, Novate Mezzola, and Gallivaggio) exceed typical values reported in the literature and thus indicate reduced mobility of the main rockfall deposit. This is partially compensated by the ejection of a volumetrically limited number of small fragments beyond the main deposit. The energy-consuming nature of the fragmentation process may be responsible for reduced main rockfall body runout. We interpret the ejection of fragments with random directions at impact to be related to the increased lateral dispersion observed for rockfalls with fragmentation. Concerning the dispersion angles of falling rock blocks, this study has practical applications for understanding rockfall dynamics: incorporating this mobility indicator could enhance the ability to assess rockfall hazards in terms of propagation. Collectively, these three field indicators of fragmentation offer tools to investigate both modern and historical rockfall events, furthering our understanding of rockfall processes and improving design of rockfall protection measures and other risk mitigation strategies.

Table 6
Summary table of proposed indicators to identify the occurrence of fragmentation.

	Trend reversion of blocks size with distance	Multifractal behavior in the frequency-volume distribution	Reduced mobility and lateral-dispersion increase of the trajectories
Villeneuve (ITA)	N	N	N
Saint-Oyen (ITA)	N	N	N
Càrcavos (ES)	N	N	N
Parkline (USA)	N	Y	Y (mobility), N (dispersion)
El Capitan (USA)	Y	Y	Y
Novate Mezzola (ITA)	Y	Y	Y
Gallivaggio (ITA)	Y	Y	Y

CRediT authorship contribution statement

Camilla Lanfranconi: Writing – review & editing, Writing – original draft, Methodology, Investigation, Formal analysis, Data curation, Conceptualization. **Paolo Frattini:** Writing – review & editing, Writing – original draft, Validation, Supervision, Methodology, Investigation, Data curation, Conceptualization. **Federico Agliardi:** Writing – review & editing, Visualization, Validation, Supervision, Methodology, Formal analysis. **Greg M. Stock:** Writing – review & editing, Writing – original draft, Supervision, Methodology, Investigation, Formal analysis. **Brian D. Collins:** Writing – review & editing, Writing – original draft, Supervision, Methodology, Investigation, Formal analysis. **Giovanni Crosta:** Writing – review & editing, Writing – original draft, Visualization, Validation, Supervision, Methodology, Conceptualization.

Declaration of competing interest

The authors declare that they have no known competing financial interests or personal relationships that could have appeared to influence the work reported in this paper.

Data availability

Data will be made available on request.

Acknowledgments

We thank Simone Demonti and Fausto Nonini for supporting the mapping of blocks, and Davide Bertolo (Regione Valle d'Aosta, Italy), Massimo Ceriani (Regione Lombardia, Italy), Luca dei Cas (ARPA Lombardia, Italy), and Roberto Sarro (IGME, Spain) for making available post-event orthophotos. We are grateful to the U.S. Geological Survey's internal reviewer Eric Bilderback for carefully reviewing the manuscript.

Additionally, we extend our thanks to the three anonymous reviewers of the journal for their feedback. Any use of trade, firm, or product names (including images) is for descriptive purposes only and does not imply endorsement by the University of Milano – Bicocca or the U.S. Government, nor discrimination against similar brands, products or services not mentioned. Due to image rights restrictions, those interested need to request access.

Appendix A. Supplementary data

Supplementary data to this article can be found online at https://doi.org/10.1016/j.enggeo.2024.107704.

References

Agliardi, F., Crosta, G.B., Frattini, P., 2009. Integrating rockfall risk assessment and countermeasure design by 3D modelling techniques. Nat. Hazards Earth Syst. Sci. 9, 1059. Katlenburg-Lindau.

Azzoni, A., La Barbera, G., Zaninetti, A., 1995, October. Analysis and prediction of rockfalls using a mathematical model. In: International Journal of Rock Mechanics and Mining Sciences & Geomechanics Abstracts, 32. Pergamon, pp. 709–724. No. 7.

Carbonneau, P.E., Bergeron, N., Lane, S.N., 2005. Automated grain size measurements from airborne remote sensing for long profile measurements of fluvial grain sizes. Water Resour. Res. 41 (11).

Collins, B.D., Corbett, S.C., Horton, E.J., Gallegos, A.J., 2022. Rockfall kinematics from massive rock cliffs: outlier boulders and flyrock from Whitney Portal, California, Rockfalls. Environ. Eng. Sci. 28 (1), 3–24.

Copons, R., Vilaplana, J.M., Linares, R., 2009. Rockfall travel distance analysis by using empirical models (Solà d'Andorra la Vella, Central Pyrenees). Nat. Hazards Earth Syst. Sci. 9 (6), 2107–2118.

Corominas, J., 1996. The angle of reach as a mobility index for small and large landslides. Can. Geotech. J. 33 (2), 260–271.

Corominas, J., Mavrouli, O., Santana, D., Moya, J., 2012. Simplified approach for obtaining the block volume distribution of fragmental rockfalls. In: Eberhardt, E., Froese, C., Turner, A.K., Leroueil, S. (Eds.), Landslides and Engineered Slopes, 2, pp. 1159–1164.

Corominas, J., Mavrouli, O., Ruiz-Carulla, R., 2017a. Rockfall occurrence and fragmentation. In: Sassa, K., Mikoš, M., Yin, Y. (Eds.), Advancing Culture of Living with Landslides. World Landslide Forum, WLF 2017, Ljubljana. Springer, Cham, pp. 75–97. https://doi.org/10.1007/978-3-319-59469-9_4.

Corominas, J., Lantada, N., Gili, J., Ruiz, R., Matas, G., Mavrouli, O., Núñez-Andrés, M. A., Moya, J., Buill, F., Abellán, A., Puig-Polo, C., Prades, A., Martinez-Bofill, J., Salo, L., 2017b. The RockRisk project: rockfall risk quantification and prevention. In: Proceedings of ROCEXS 2017, 6th Interdisciplinary Workshop on Rockfall Protection, May 2017, Barcelona (Spain), pp. 39–42. Available at: http://congress.cimne.com/rocexs2017/frontal/Doc/Ebook.pdf.

Crosta, G.B., Agliardi, F., 2004. Parametric evaluation of 3D dispersion of rockfall trajectories. Nat. Hazards Earth Syst. Sci. 4 (4), 583–598.

Crosta, G.B., Agliardi, F., Frattini, P., Imposimato, S., 2004. A three-dimensional hybrid numerical model for rockfall simulation. In: Geophys Res Abstr, 6, p. 04502.

Crosta, G.B., Frattini, P., Fusi, N., 2007. Fragmentation in the Val Pola rock avalanche, Italian alps. J. Geophys. Res. Earth 112 (F1).

Crosta, G.B., Agliardi, F., Frattini, P., Lari, S., 2015. Key issues in rock fall modeling, hazard and risk assessment for rockfall protection. In: Engineering Geology for Society and Territory, Vol. 2.

Crosta, G.B., De Blasio, F.V., Frattini, P., 2018. Global scale analysis of Martian landslide mobility and paleoenvironmental clues. J. Geophys. Res. Planets 123 (4), 872–891.

Cruden, D.M., Varnes, D.J., 1996. Landslide types and processes. In: Turner, A.K., Schuster, R.L. (Eds.), Landslide Investigation and Mitigation. Special Report 247, 3. Transportation Research Board, US National Research Council, Washington, DC, pp. 36–75.

Davies, T.R., McSaveney, M.J., 2009. The role of rock fragmentation in the motion of large landslides. Eng. Geol. 109 (1–2), 67–79.

Davies, T.R., McSaveney, M.J., Hodgson, K.A., 1999. A fragmentation-spreading model for long-runout rock avalanches. Can. Geotech. J. 36 (6), 1096–1110.

De Biagi, V., Napoli, M.L., Barbero, M., 2017. A quantitative approach for the evaluation of rockfall risk on buildings. Nat. Hazards 88, 1059–1086.

De Blasio, F.V., Crosta, G.B., 2015. Fragmentation and boosting of rock falls and rock avalanches. Geophys. Res. Lett. 42 (20), 8463–8470.

De Blasio, F.V., Dattola, G., Crosta, G.B., 2018. Extremely energetic rockfalls. J. Geophys. Res. Earth 123 (10), 2392–2421.

Dei Cas, L., Pastore, M.L., Rivolta, C., 2018. Gallivaggio landslide: the geological monitoring, of a rock cliff, for early warning system. Ital. J. Eng. Geol. Environ 18, 41–55.

Dussauge, C., Grasso, J.R., Helmstetter, A., 2003. Statistical analysis of rockfall volume distributions: Implications for rockfall dynamics. J. Geophys. Res. Solid Earth 108 (B6).

Dussauge-Peisser, C., Helmstetter, A., Grasso, J.R., Hantz, D., Desvarreux, P., Jeannin, M., Giraud, A., 2002. Probabilistic approach to rock fall hazard assessment: potential of historical data analysis. Nat. Hazards Earth Syst. Sci. 2 (1/2), 15–26.

EU-DEM, 2016. European Digital Elevation Model, EU-DEM (raster) – version 1.1, Apr. 2016 (Temporal Coverage 2010-2011). European Environment Agency. https://www.eea.europa.eu/en/datahub/datahubitem-view/d08852bc-7b5f-4835-a776-08362e2fbf4b (last accessed on June 6, 2024).

Evans, S.G., Hungr, O., 1993. The assessment of rockfall hazard at the base of Talus Slopes. Can. Geotech. J. 30, 620–636.

Fallot, P., 1948. Les cordilléres betiques. Imprenta Elzeviriana, Sablons, France.

Frattini, P., Crosta, G.B., Agliardi, F., Clague, J.J., Stead, D., 2012. 22 Rockfall characterization and modeling. In: Landslides: Types, Mechanisms and Modeling, 267.

Gallo, I.G., Martínez-Corbella, M., Sarro, R., Iovine, G., López-Vinielles, J., Hérnandez, M., Robustelli, G., Mateos, R.M., García-Davalillo, J.C., 2021. An integration of UAV-based photogrammetry and 3D modelling for rockfall hazard assessment: the Cárcavos case in 2018 (Spain). Remote Sens. 13 (17), 3450.

Guerin, A., Stock, G.M., Radue, M.J., Jaboyedoff, M., Collins, B.D., Matasci, B., Avdievitch, N., Derron, M.H., 2020. Quantifying 40 years of rockfall activity in Yosemite Valley with historical Structure-from-Motion photogrammetry and terrestrial laser scanning. Geomorphology 356, 107069.

Hantz, D., Corominas, J., Crosta, G.B., Jaboyedoff, M., 2021. Definitions and concepts for quantitative rockfall hazard and risk analysis. Geosciences 11 (4), 158.

Haug, Ø.T., Rosenau, M., Leever, K., Oncken, O., 2016. On the energy budgets of fragmenting rockfalls and rockslides: insights from experiments. J. Geophys. Res. Earth 121 (7), 1310–1327.

Heim, A., 1932. Bergsturz und Menschenleben. Beiblatt zur Vierteljahrsschrift der Naturforschenden Gesellschaft in Zurich, 77, pp. 1–217. Translated by N. Skermer under the title Landslides and Human Lives, BiTech Publishers, Vancouver, British Columbia, 1989, p. 195. Hungr, O., Evans, S. G., & Hazzard, J. (1999). Magnitude and frequency of rock falls and rock slides along the main transportation corridors of southwestern British Columbia. Canadian Geotechnical Journal, 36(2), 224–238.

Hungr, O., Leroueil, S., Picarelli, L., 2014. The Varnes classification of landslide types, an update. Landslides 11, 167–194.

Hunter, G., Fell, R., 2003. Travel distance angle for" rapid" landslides in constructed and natural soil slopes. Can. Geotech. J. 40 (6), 1123–1141.

IGME, 2024. Instituto Geológico y Minero de España. https://www.igme.es/ (last accessed on June 6, 2024).

Jaboyedoff, M., Dudt, J.P., Labiouse, V., 2005. An attempt to refine rockfall hazard zoning based on the kinetic energy, frequency and fragmentation degree. Nat. Hazards Earth Syst. Sci. 5 (5), 621–632.

Jin, K., Xing, A., Li, B., He, K., Zhuang, Y., Chang, W., 2023. Dynamic fragmentation characteristics of columnar rockfall: insights from discrete element method. Bull. Eng. Geol. Environ. 82 (8), 322.

Lanfranconi, C., Sala, G., Frattini, P., Crosta, G.B., Valagussa, A., 2020. Assessing the rockfall protection efficiency of forests at the regional scale. Landslides 17, 2703–2721.

Lanfranconi, C., Frattini, P., Sala, G., Dattola, G., Bertolo, D., Sun, J., Crosta, G.B., 2023. Accounting for the effect of forest and fragmentation in probabilistic rockfall hazard. Nat. Hazards Earth Syst. Sci. 23 (6), 2349–2363.

Lari, S., Frattini, P., Crosta, G.B., 2014. A probabilistic approach for landslide hazard analysis. Eng. Geol. 182, 3–14.

Locat, P., Couture, R., Leroueil, S., Locat, J., Jaboyedoff, M., 2006. Fragmentation energy in rock avalanches. Can. Geotech. J. 43 (8), 830–851.

Lombardia, Regione, 2024. Geoportale della Lombardia, Digital Terrain Model and shaded relief maps of the Gallivaggio and Novate Mezzola case studies. https://www.geoportale.regione.lombardia.it/ (last accessed on March 25, 2024).

Malamud, B.D., Turcotte, D.L., Guzzetti, F., Reichenbach, P., 2004. Landslide inventories and their statistical properties. Earth Surf. Process. Landf. 29 (6), 687–711.

Massey, C.I., Gerstenberger, M., McVerry, G., Litchfield, N., 2012. Canterbury Earthquakes 2010/11 Port Hills Slope Stability: Additional Assessment of the Life-safety Risk From Rockfalls (Boulder Rolls).

Matas, G., Lantada, N., Corominas, J., Gili, J.A., Ruiz-Carulla, R., Prades, A., 2017. RockGIS: a GIS-based model for the analysis of fragmentation in rockfalls. Landslides 14 (5), 1565–1578.

Menegoni, N., Giordan, D., Perotti, C., 2020. Reliability and uncertainties of the analysis of an unstable rock slope performed on RPAS digital outcrop models: The case of the gallivaggio landslide (Western Alps, Italy). Remote Sens. 12 (10), 1635.

NPS, 2024. Yosemite National Park Rockfall Database (1857–2023), 12 June 2017 Parkline Rockfall. https://experience.arcgis.com/experience/03e5fb490eaf4bef92494923a99c4fa0/page/2D-Map-of-rock-falls/.

Quantum Spatial, 2020. Yosemite National Park, California 3DEP Lidar Technical Data Report Contract no. G16PC00016, Task Order No. 140G0219F0292, p. 35. https://prd-tnm.s3.amazonaws.com/StagedProducts/Elevation/metadata/CA_YosemiteNP_2019_D19/CA_YosemiteNP_2019/reports/Yosemite_California_NIR_Lidar_Technical_Data_Report.pdf (accessed June 3, 2024).

Rapp, A., 1960. Recent development of mountain slopes in Kärkevagge and surroundings, northern Scandinavia. Geogr. Ann. 42 (2–3), 65–200.

Regione Autonome Vallee d''Aosta, 2024. Geoportale, Digital Terrain Model and shaded relief maps of the Villeneuve and Saint-Oyen case studies. https://geoportale.regione.vda.it/ (last accessed on March 25, 2024).
Ruiz-Carulla, R., Corominas, J., Mavrouli, O., 2015. A methodology to obtain the block size distribution of fragmental rockfall deposits. Landslides 12 (4), 815–825.
Ruiz-Carulla, R., Corominas, J., Mavrouli, O., 2018. Comparison of block size distribution in rockfalls. In: Landslides and Engineered Slopes. Experience, Theory and Practice. CRC Press, pp. 1767–1774.
Sala, Z., Hutchinson, D.J., Harrap, R., 2019. Simulation of fragmental rockfalls detected using terrestrial laser scans from rock slopes in south-Central British Columbia, Canada. Nat. Hazards Earth Syst. Sci. 19, 2385–2404. https://doi.org/10.5194/nhess-19-2385-2019.
Scheidegger, A.E., 1973. On the prediction of the reach and velocity of catastrophic landslides. Rock Mech. 5 (4), 231–236.
Stock, G.M., Guerin, A., Avdievitch, N., Collins, B.D., Jaboyedoff, M., 2018. Rapid 3-D analysis of rockfalls. GSA Today 28 (8), 28–29.
Strunden, J., Ehlers, T.A., Brehm, D., Nettesheim, M., 2015. Spatial and temporal variations in rockfall determined from TLS measurements in a deglaciated valley, Switzerland. J. Geophys. Res. Earth Surf. 120, 1251–1273. https://doi.org/10.1002/2014JF003274.
USDA, 2024. U.S. Department of Agriculture, National Agriculture Imagery Program - NAIP Hub Site (arcgis.com) (accessed 10 May 2024).
Volkwein, A., Roth, A., Gerber, W., Vogel, A., 2009. Flexible rockfall barriers subjected to extreme loads. Struct. Eng. Int. 19 (3), 327–332.
Walton, W.H., 1948. Feret's statistical diameter as a measure of particle size. Nature 162 (4113), 329–330.
Wang, X., Frattini, P., Crosta, G.B., Zhang, L., Agliardi, F., Lari, S., Yang, Z., 2014. Uncertainty assessment in quantitative rockfall risk assessment. Landslides 11, 711–722.
Whalley, W.B., 1974. The mechanics of high magnitude, low frequency rock failure and its importance in a mountainous area. Geogrl. Papers. Read. 27, 48.
Wieczorek, G.F., Morrissey, M.M., Iovine, G., Godt, J., 1998. Rockfall hazards in the Yosemite Valley. US Geol. Survey Open-File Report 98 (467), 8.
Woodget, A.S., Austrums, R., 2017. Subaerial gravel size measurement using topographic data derived from a UAV-SfM approach. Earth Surf. Process. Landf. 42 (9), 1434–1443.
Zhao, T., Crosta, G.B., Utili, S., De Blasio, F.V., 2017. Investigation of rock fragmentation during rockfalls and rock avalanches via 3-D discrete element analyses. J. Geophys. Res. Earth 122 (3), 678–695.